Check for updates

Construction and characterization of a magnetic nanoparticle-supported Cu complex: a stable and active nanocatalyst for synthesis of heteroaryl–aryl and di-heteroaryl sulfides†

Yutong Fang,[a] Songlin Chen*[bc] and Li-Yuan Chang [ID] *[d]

Diaryl and di-heteroaryl sulfides exist in the structure of many drugs and important biological compounds, also these compounds are well-known in medicinal chemistry due to important biological and pharmaceutical activities. Therefore, the development of novel, ecofriendly and efficient catalytic systems for the preparation of diaryl and di-heteroaryl sulfides is a very attractive and important challenge in organic synthesis. In this attractive methodology, we wish to introduce Fe_3O_4-supported 3-amino-4-mercaptobenzoic acid copper complex (Fe_3O_4@AMBA-CuI) nanomaterials as a novel and efficient magnetically recoverable catalyst for the preparation of heteroaryl-aryl and di-heteroaryl sulfides with high yields through reaction of heteroaryl halides with aryl or heteroaryl boronic acids and S_8 as the sulfur source under ecofriendly conditions. This catalytic system was very efficient and practical for a diverse range of heteroaryl substrates including benzothiazole, benzoxazole, benzimidazole, oxadiazole, benzofuran, and imidazo[1,2-*a*]pyridine, because the desired diaryl and di-heteroaryl sulfides were prepared with high yields. The reusability-experiments revealed that the Fe_3O_4@AMBA-CuI nanocatalyst can be magnetically separated and reused at least six times without a significant decrease in its catalytic activity. VSM and ICP-OES analyses confirmed that despite using the Fe_3O_4@AMBA-CuI nanocatalyst 6 times, the magnetic properties and stability of the catalyst were still maintained. Although all the obtained heteroaryl-aryl and di-heteroaryl sulfide products are known and previously reported, the synthesis of this number of heteroaryl-aryl and di-heteroaryl sulfides has never been reported by any previous methods.

Introduction

Catalysts are one of the key factors or reagents of most chemical transformations.[1] Most industrial and chemical processes and almost all chemical reactions require catalysts.[2–4] Generally, catalysts are divided into two large categories, homogeneous and heterogeneous catalysts.[5,6] Homogeneous catalysts show more activity than heterogeneous catalysts due to their high dispersion.[7–10] But the main problem in homogeneous catalysts is their difficult separation from the reaction mixture, often associated with the production of large amounts of waste and high energy consumption.[11–13] But in heterogeneous catalysis

systems, the problem of catalyst separation can be solved by simple methods such as centrifugation.[14] Therefore, the best catalytic system is one that has the advantages of both homogeneous and heterogeneous catalysts.[15] Stabilization of the desired catalyst on a solid substrate was considered as an ideal solution to prepare efficient and green catalysts.[16–19] In the new century, all eyes turned towards nanotechnology in catalyst science because nanoparticles have valuable properties.[20–22] In the last decade, the immobilization of transition metals on nanoparticles to prepare an environmentally friendly, separable and efficient catalyst has been used as a popular catalytic system.[23–25] Heterostructure/hybrid catalysts offer a compelling array of advantages, prominently characterized by their ability to amalgamate the distinctive merits of individual components.[26,27] By fusing different materials into a heterostructure, these catalysts harness a synergistic effect that enhances overall performance. One key advantage lies in the combination of complementary properties, allowing for the optimization of catalytic activity through the cooperative interaction of diverse components.[28,29] This integration facilitates improved reactivity, efficient charge transfer, and, consequently, heightened

[a]Sinopec Research Institute of Petroleum Processing, Beijing 100089, China
[b]Department of Basics, Naval University of Engineering, Wuhan 430030, Hubei, China. E-mail: chensonglin0170@163.com
[c]School of Resource and Environmental Engineering, Wuhan University of Science and Technology, Wuhan 430070, Hubei, China
[d]Institute of Chemical and Nanotechnology Research, Shanghai, China. E-mail: liyuanchang839@gmail.com

catalytic efficiency.[30,31] Heterostructure catalysts, exemplified by their capacity to merge the strengths of varied materials, transcend the limitations of traditional catalysts.[32,33] The versatility inherent in these catalysts enables their customization for specific reactions, contributing to their applicability across a wide range of chemical processes.[34–36] In essence, the advantages of heterostructure/hybrid catalysts lie in their ability to go beyond the capabilities of individual components, offering a versatile and efficient platform for catalyzing diverse reactions in the realm of materials science and chemical engineering.

Among nanomaterials, magnetic nanoparticles have attracted the attention of many researchers in catalysis processes due to their unique characteristics.[37,38] During the last decade, the research on catalytic application of magnetic nanoparticles has been studied significantly and it is due to its simple synthesis, low cost and relatively high sensitivity.[39–42] An outstanding feature of the catalysts immobilized on the magnetic nanoparticles is that they are easily separated from the reaction environment by applying an external magnetic field.[43,44] Surface modification of magnetic nanoparticles is usually done easily and the synthesized nanomagnetic-catalyst has high stability and efficiency and is easily separated from the reaction mixture.[45–47]

Research on coupling reactions is always a very attractive and ideal challenge for chemists because these reactions are usually difficult and under harsh conditions.[48,49] One of the most popular reactions in this field is research on the formation of sulfur-carbon bonds (sulfides) through C–S coupling reactions.[50,51] Sulfides are organic compounds that have a wide variety of applications in organic chemistry, medicine, and biochemistry.[52–54] In addition, many natural compounds, amino acids and enzymes of living organisms either have C–S bonds or are used for the synthesis of sulfides.[55] Diaryl and di-heteroaryl sulfides are an important category of compounds containing

C–S bonds that have important medicinal properties such as anti-inflammatory, treatment of diabetes, Alzheimer's, Parkinson's disease or as an inhibitor for the treatment of human immunodeficiency virus, asthma, obstructive pulmonary disease, platelet aggregation inhibitors or anti-cancer.[56–59] Diaryl and heteroaryl sulfides exist in the structure of many drugs and important biological compounds, some examples of which are shown in Fig. 1.[59–62] So far, many methods have been reported for the preparation of diaryl sulfides, but most of these methods, despite their advantages, also have a series of disadvantages, such as the use of expensive catalysts, toxic solvents, difficult reaction conditions, and long time.

As Cu based catalysts are the most efficient catalysts in this process, in this attractive methodology, we wish to introduce AMBA-CuI functionalized Fe_3O_4 nanomaterials as a novel and efficient magnetically recoverable catalyst for the preparation of heteroaryl-aryl and di-heteroaryl sulfides with high yields through reaction of heteroaryl halides with aryl or heteroaryl boronic acids and S_8 as sulfur source under ecofriendly conditions.

Result and discussion

Preparation of Fe_3O_4@AMBA-CuI nanocatalyst

The stepwise preparation of Fe_3O_4@AMBA-CuI nanocatalyst is shown in Scheme 1. First, magnetic Fe_3O_4 nanoparticles coated with 3-amino-4-mercaptobenzoic acid (AMBA) in order to fabricate Fe_3O_4@AMBA nanomaterial as ligand. Then, CuI was immobilized on the Fe_3O_4@AMBA ligand at refluxing ethanol to construct Fe_3O_4@AMBA-CuI nanocatalyst.

Characterization of Fe_3O_4@AMBA-CuI nanocatalyst

The structure of Fe_3O_4@AMBA-CuI nanocatalyst was well characterized with a number of spectroscopic techniques.

HIV-1 Integrase Inhibitor

nicotinic acetylcholine receptor ligand

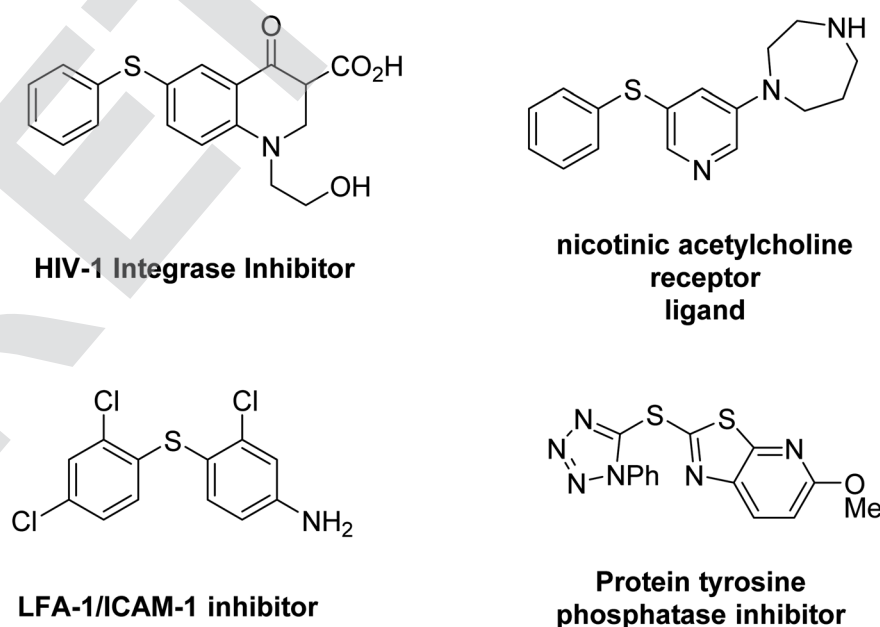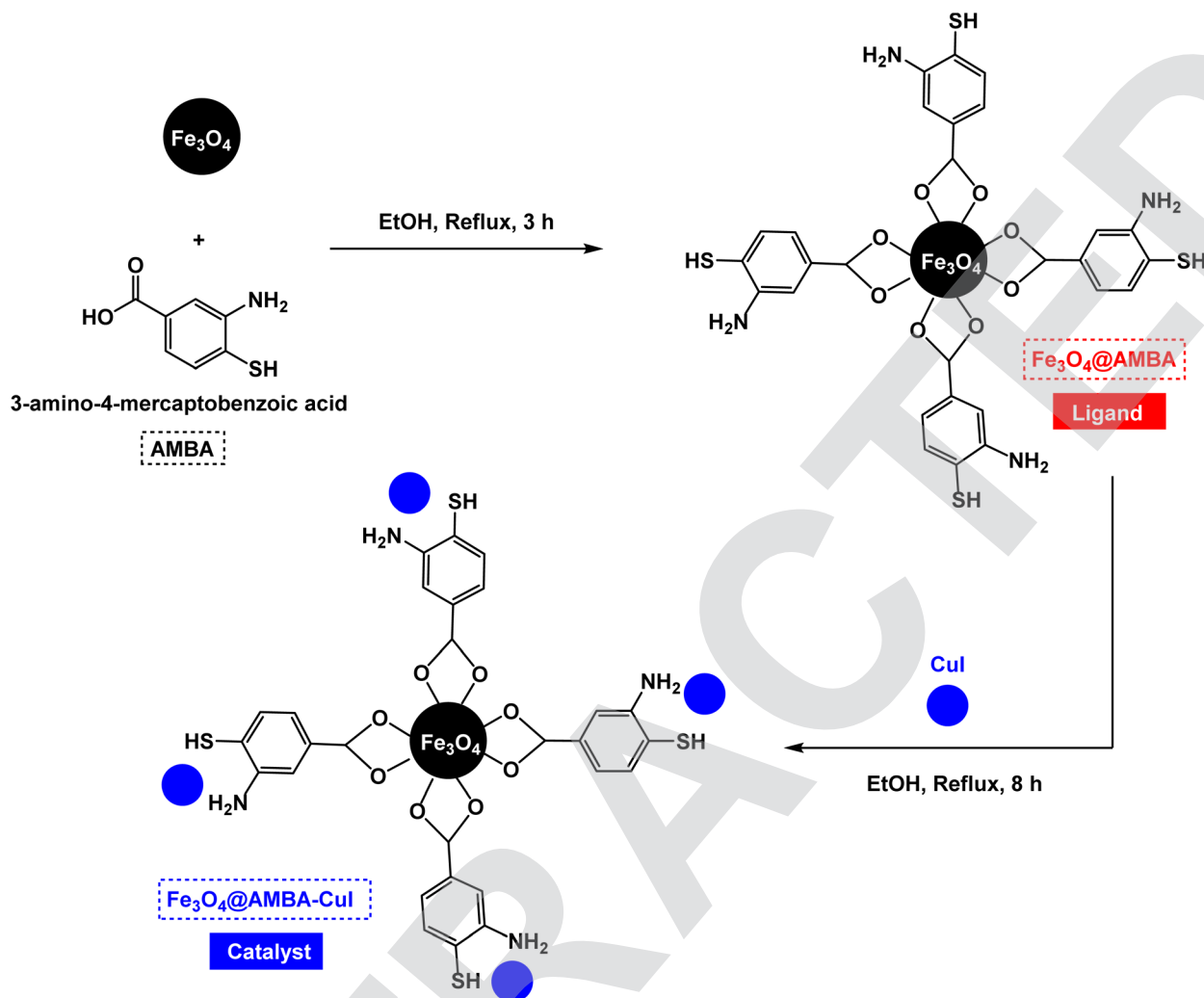**LFA-1/ICAM-1 inhibitor**

Protein tyrosine phosphatase inhibitor

Fig. 1   Valuable biological and bioactive molecules with diaryl or heteroaryl sulfide structure.

Scheme 1 General schematic for fabrication of Fe$_3$O$_4$@AMBA-CuI nanocatalyst.

FT-IR spectroscopy. In order to understand functional groups supported on magnetic nanoparticles, FT-IR spectra of Fe$_3$O$_4$@AMBA ligand and Fe$_3$O$_4$@AMBA-CuI nanocatalyst was taken. As shown in Fig. 2, the presence of a specific peak in the region of 580 cm^{-1} confirms the iron–oxygen bond. The presence of hydroxyl groups was determined by the broad peak in the region of approximately 3400 cm^{-1}. Also, the presence of a broad peak in the region of 2800–3000 cm^{-1} is related to C–H
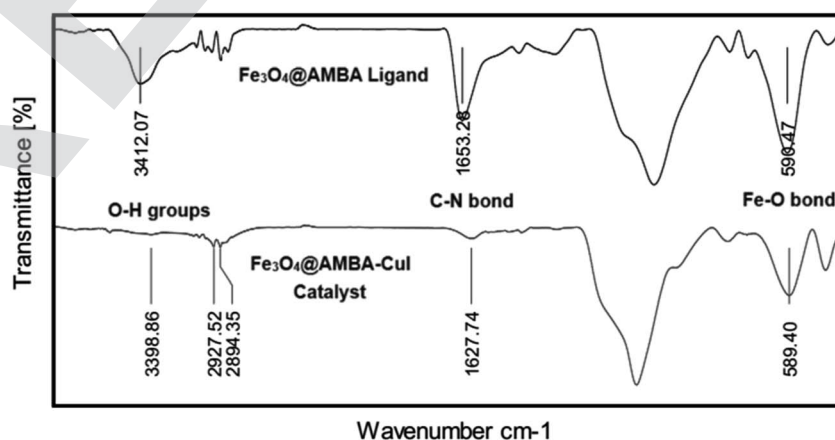
Fig. 2 FT-IE spectra of Fe$_3$O$_4$@AMBA ligand and Fe$_3$O$_4$@AMBA-CuI nanocatalyst.
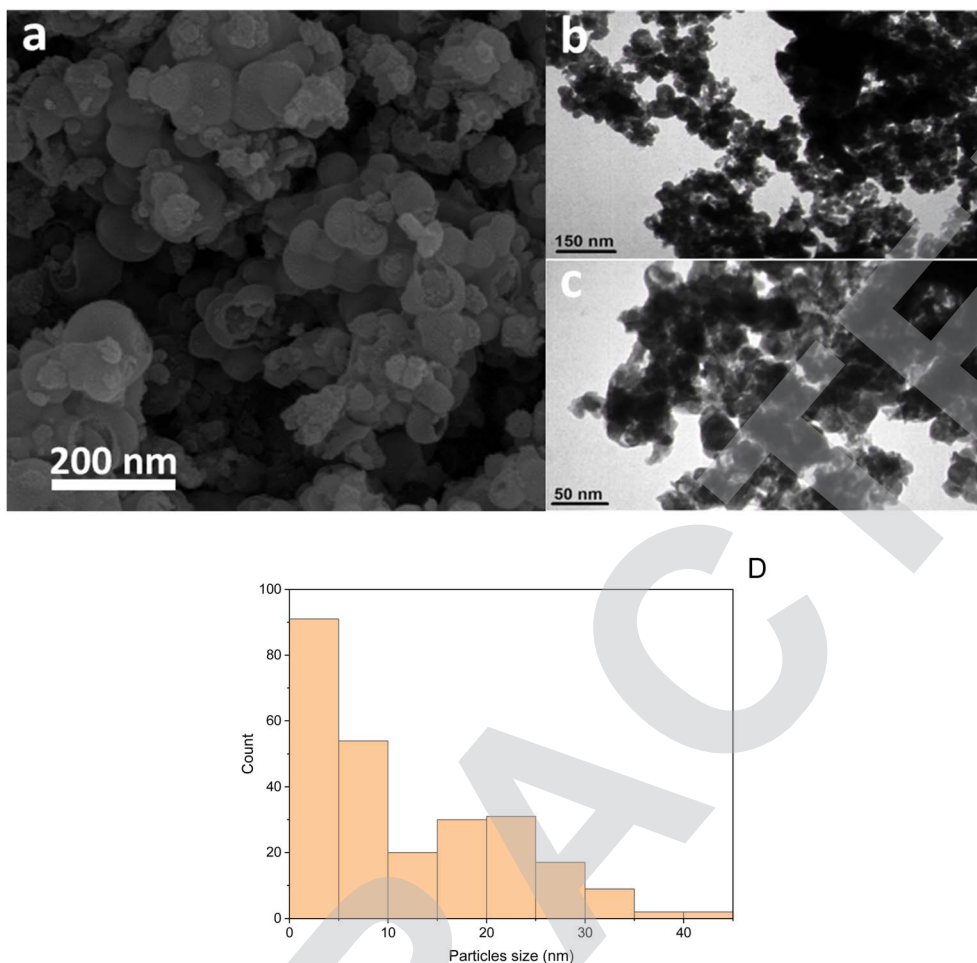
Fig. 3 (a) SEM, (b and c) TEM images of Fe$_3$O$_4$@AMBA-CuI nanocatalyst at different magnifications and (d) particles distribution histogram.

bonds in aromatic ring. The peak related to the C–N bond was observed in the region of 1630 cm^{-1}. Compared to the spectrum of the Fe$_3$O$_4$@AMBA ligand, the C–N peak in the catalyst shifted to the lower region (1627 cm^{-1}), which indicates the fixation of copper metal on the ligand.

SEM and TEM analysis. The morphology and structure of particles in Fe$_3$O$_4$@AMBA-CuI nanocatalyst was studied by SEM and TEM photographs. The SEM and TEM images clearly showed that the formed particles are spherical and uniform and their size is in the range of nanometers. TEM images and histogram shown that the particles have a size in the range of 20 nm Fig. 3.

EDX, elemental mapping and ICP-OES analysis. In order to understand the elements in the Fe$_3$O$_4$@AMBA-CuI nanocatalyst structure, EDX and elemental mapping techniques were used (Fig. 4 and 5). These techniques confirmed the presence of Fe (47.31 wt%), and O (32.34 wt%), as the main elements of Fe$_3$O$_4$ catalytic support, in addition the presence of C (12.81 wt%), N (3.54 wt%), S (2.73 wt%) and Cu (1.27 wt%) in the structure confirm the formation of Fe$_3$O$_4$@AMBA-CuI nanocatalyst. It is worth to mention that the distribution pattern of Cu species is in excellent with the nitrogen and sulfur species on catalyst surface that confirm their correlation and complexation. ICP-

OES analysis was used to find out the amount of copper in the structure of the Fe$_3$O$_4$@AMBA-CuI nanocatalyst, and the results showed that the amount of Cu in the structure of the nanocatalyst is 14.32×10^{-5} mol g^{-1} which confirm the presence of copper in structure and successful complexation of surface functionalities with the Cu ions.
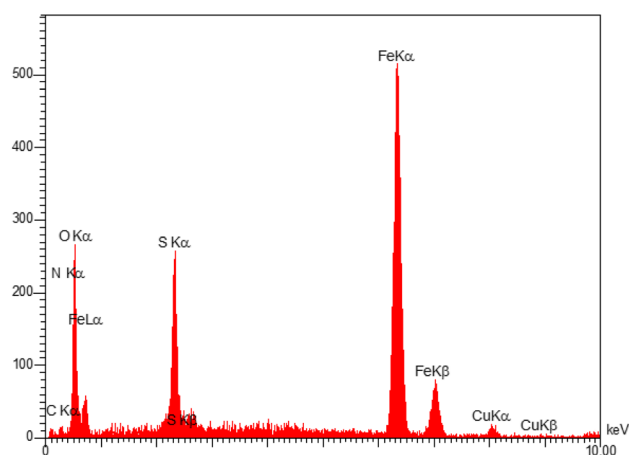

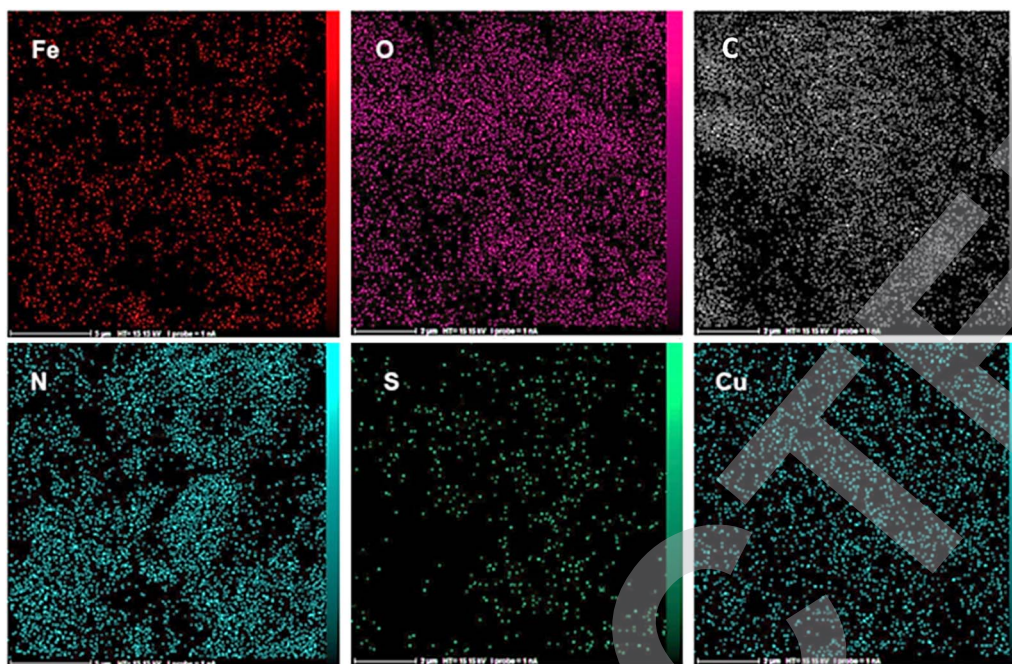**Fig. 4** EDX analysis of Fe$_3$O$_4$@AMBA-CuI nanocatalyst.

Fig. 5 The X-ray map analysis of Fe$_3$O$_4$@AMBA–CuI nanocatalyst.
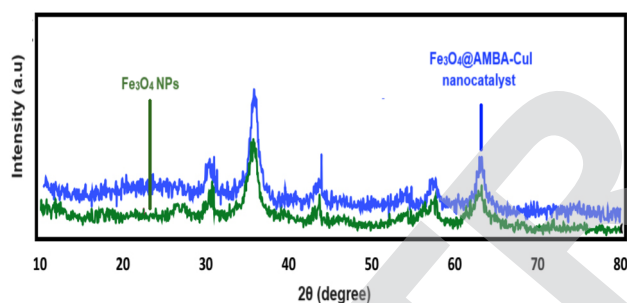
Fig. 6 XRD analysis of Fe$_3$O$_4$ NPs and Fe$_3$O$_4$@AMBA–CuI nanocatalyst.

XRD analysis. In order to study the structure and nature of Fe$_3$O$_4$ and Fe$_3$O$_4$@AMBA-CuI nanocatalyst, XRD analysis were used. XRD spectra of Fe$_3$O$_4$ NPs and Fe$_3$O$_4$@AMBA-CuI nanocatalyst are shown in Fig. 6. As was found in XRD analysis, the first inner layer "Fe$_3$O$_4$" core was properly synthesized which its cubic pattern of the crystallography, is in agreement with standard magnetic XRD spectra and "9 005 840" COD. The XRD patterns shows peaks in 30.35°, 35.535°, 37.26°, 43.33°, 47.20°, 53.50°, 57.15°, 62.8° and 64.90° which are assigned by miller indices 220, 311, 222, 400, 331, 422, 511, 440, and 531 respectively.[63] As you can see in the X-ray analysis, the spectra of the Fe$_3$O$_4$@AMBA-CuI nanocatalyst and the magnetic Fe$_3$O$_4$ nanoparticles completely coincide, which indicates that the nature of the Fe$_3$O$_4$@AMBA-CuI catalyst has not changed despite the immobilization of the 3-amino-4-mercaptobenzoic acid (AMBA) and CuI on the surface of magnetic Fe$_3$O$_4$ nanoparticles.

TGA analysis. To assess the thermal stability of the Fe$_3$O$_4$@AMBA-CuI nanocatalyst, we employed Thermogravimetric Analysis (TGA) with air as the oxygen atmosphere. The TGA spectra of the Fe$_3$O$_4$@AMBA-CuI nanocatalyst are illustrated in Fig. 7. A discernible decrease in weight, approximately 5%, was observed below 225 °C. This phenomenon is ascribed to the elimination of physically or chemically adsorbed water from the catalyst surface, aligning with findings from previous Fe$_3$O$_4$ TGA studies.[64,65] Consistent with literature reports, the TGA curve for bare Fe$_3$O$_4$ tends to stabilize above 200 °C, denoting the completion of primary thermal events.[65–67] The residual mass signifies the presence of remaining iron oxide products or any inert material within the sample.[68,69] Notably, the TGA analysis of the Fe$_3$O$_4$@AMBA-CuI nanocatalyst revealed an additional substantial weight loss between 225 and 600 °C. This aligns with expectations for the region where organic contaminants or impurities undergo decomposition through aerobic pyrolysis.[70] In this instance, the weight loss is attributed to the degradation of AMBA moieties on the surface of Fe$_3$O$_4$ MNPs, validating the successful synthesis of the target complex *via* post-modification methods.

VSM analysis. The magnetic property of the Fe$_3$O$_4$@AMBA-CuI nanocatalyst was measured by vibrating-sample magnetometer (VSM) analysis. As shown in Fig. 8, VSM analysis showed that the Fe$_3$O$_4$@AMBA-CuI catalyst has a magnetic property of 46.721 emu g^{-1}, which confirms that despite the immobilization of 3-amino-4-mercaptobenzoic acid (AMBA) and CuI on the surface of the magnetic nanoparticles, it still has a high magnetic property.

Catalytic investigation in heteroaryl-aryl and di-heteroaryl sulfide products

After identifying the structure of the Fe$_3$O$_4$@AMBA-CuI catalyst, we decided to investigate its catalytic activity in the C–S coupling reactions. First, one-pot three-component reaction of
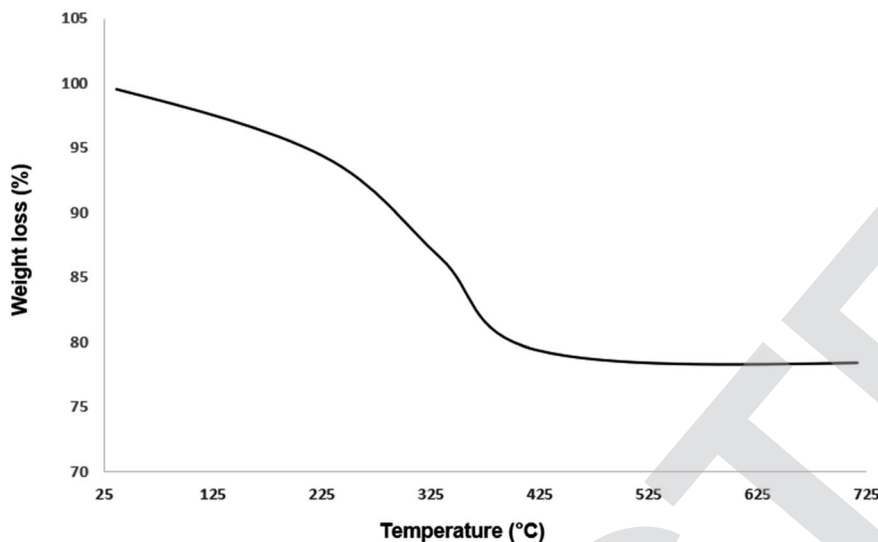
Fig. 7 TGA analysis of Fe_3O_4@AMBA–CuI nanocatalyst.

2-iodobenzo[*d*]thiazole with phenyl boronic acid and S_8 as sulfur source was optimized under different conditions. In the absence of catalyst, the model reaction was not performed using NaOH as base in DMF (Table 1, entry 1). With introduction of Fe_3O_4@AMBA-CuI catalyst, the 2-(phenylthio)benzo[*d*]thiazole (**product 4a**) was synthesized with good yields; and by standardizing the amount of Fe_3O_4@AMBA-CuI catalyst, the amount of 8 mol% was chosen as the optimal amount for C–S coupling reactions (Table 1, entry 6).

The presence of base for the synthesis of heteroaryl-aryl and di-heteroaryl sulfides was very vital because the 2-(phenylthio)benzo[*d*]thiazole (**product 4a**) was not formed in the absence of base (Table 2, entry 1). To find the best base, a number of conventional bases was tested and the results confirmed that potassium acetate (KOAc) is the most efficient base for the synthesis of the 2-(phenylthio)benzo[*d*]thiazole (**product 4a**) (Table 2, entry 6). Finally, in order to select the best medium reaction, a number of solvents were tested under the optimized amount of Fe_3O_4@AMBA-CuI
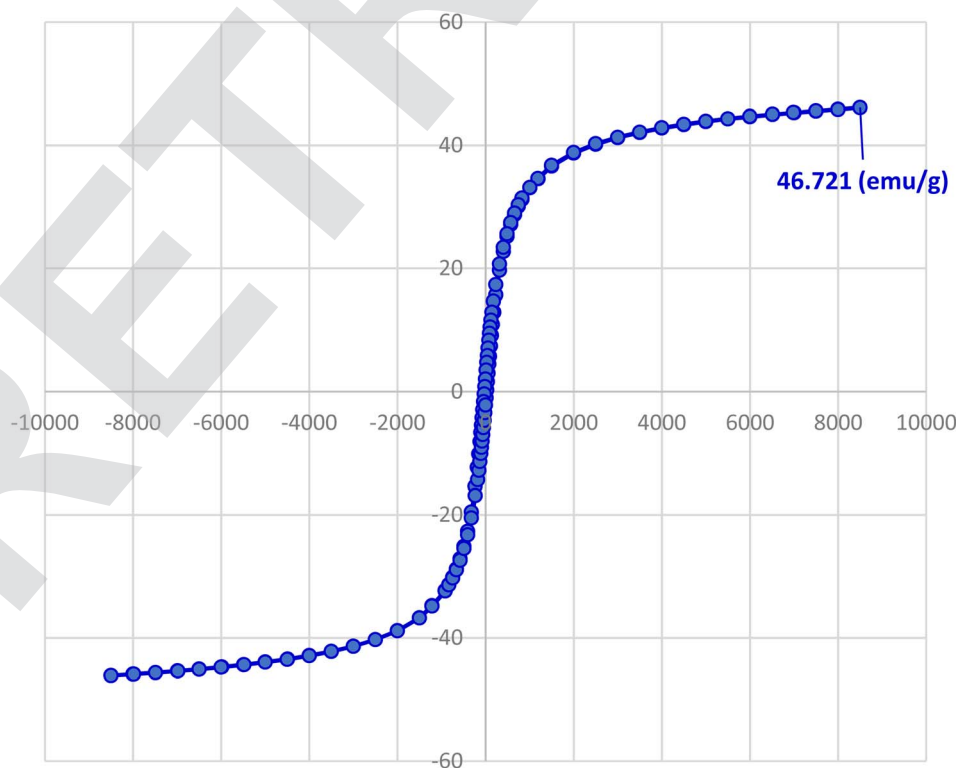

46.721 (emu/g)

Fig. 8 VSM analysis of Fe_3O_4@AMBA–CuI nanocatalyst.

Table 1 Effect of catalyst on the preparation of 2-(phenylthio)benzo[d]thiazole (**product 4a**)

Entry	Catalyst (mol%)	Time (h)	Yield%[a]
1	No catalyst	24	✖
2	Fe_3O_4 (5 mol%)	24	11%
3	Fe_3O_4@AMBA-CuI (5 mol%)	6	69%
4	Fe_3O_4@AMBA-CuI (6 mol%)	6	75%
5	Fe_3O_4@AMBA-CuI (7 mol%)	6	73%
6	**Fe_3O_4@AMBA-CuI (8 mol%)**	**6**	**86%**
7	Fe_3O_4@AMBA-CuI (9 mol%)	6	86%
8	Fe_3O_4@AMBA-CuI (10 mol%)	6	86%

[a] Yields referred to isolated products.

nanocatalyst in the presence of KOAc as base. The results confirmed that PEG is the best solvent for C–S coupling reactions. It is worth mentioning that when the reaction temperature increased from 100 to 120 °C, the yield of the obtained product increased (from 93% to 95%) and the reaction time decreased (from 6 h to 5 h) (Table 3, entry 8). But the temperature above 120 °C did not affect the progress of the reaction.

In next stage of experimental works, we decide to study the scope of heteroaryl iodides and aryl or heteroaryl boronic acids for synthesis of heteroaryl-aryl and di-heteroaryl sulfides catalyzed by Fe_3O_4@AMBA-CuI nanomaterial (8 mol%) in the presence of KOAc in PEG at 120 °C for 5 h (Table 4). As seen in Table 4, most of the heteroaryl-aryl and di-heteroaryl sulfide products were synthesized with excellent yields and the

Table 2 Effect of several base on the preparation of 2-(phenylthio)benzo[d]thiazole (**product 4a**)

Entry	Base	Time (h)	Yield%[a]
1	No base	24	✖
2	NaOH	6	86%
3	KOH	6	79%
4	t-BuOK	6	22%
5	Pyridine	6	17%
6	**KOAc**	**6**	**90%**
7	Et_3N	6	63%
8	K_2CO_3	6	87%
9	CsF	6	84%
10	DBU	6	30%

[a] Yields referred to isolated products.

Table 3 Influence of solvent and temperature on the preparation of 2-(phenylthio)benzo[d]thiazole (product 4a)

Entry	Solvent (°C)	Time (h)	Yield%[a]
1	DMF (100 °C)	6	90%
2	EtOH (reflux)	6	85%
3	Toluene (100 °C)	6	34%
4	DMSO (100 °C)	6	87%
5	Water (reflux)	6	42%
6	PEG (100 °C)	6	93%
7	PEG-400 (110 °C)	5	93%
8	**PEG-400 (120 °C)**	**5**	**95%**
9	PEG-400 (130 °C)	5	95%
10	Solvent-free (100 °C)	5	93%
11	PEG-400 (120 °C)	12	8%

[a] Yields referred to isolated products.

presence of different functional groups on the phenyl ring did not have much effect on the yield of the sulfide products. This catalytic system was very efficient and practical for a diverse range of heteroaryl iodides including benzothiazole, benzoxazole, benzimidazole, oxadiazole, benzofuran, imidazo[1,2-*a*] pyridine, because the desired diaryl and di-heteroaryl sulfides were prepared with high yields. Although all the obtained heteroaryl-aryl and di-heteroaryl sulfide products are known and previously reported, but synthesis of this number of heteroaryl-aryl and di-heteroaryl sulfides has never been reported by any methods.

Based on methods reported for preparation of diaryl sulfides in the presence of copper catalysts, we presented a plausible mechanistic-pathway for synthesis of heteroaryl-aryl and di-heteroaryl sulfides through three-component reaction of heteroaryl halides with aryl or heteroaryl boronic acids and S_8 as sulfur source catalyzed by Fe_3O_4@AMBA-CuI nanomaterial. In this respect, one-pot three-component reaction of 2-iodobenzo[*d*]thiazole with phenyl boronic acid and S_8 as sulfur source for the synthesis of **product 4a** was considered as the model reaction (Scheme 2). First, copper disulfide was prepared from the reaction of Fe_3O_4@AMBA-CuI nanocatalyst with potassium disulfide (formed the reaction of KOAc with S_8). The oxidative-addition of phenyl boronic acid to copper disulfide led to form aryl organocopper (intermediate **A**), which may convert to intermediate **B**. Then, the reaction of 2-iodobenzo[*d*]thiazole with intermediate **B** led to form key intermediate **C**, which followed a reduction-elimination process in order to prepare the 2-(phenylthio)benzo[*d*]thiazole (**Product 4a**).

Catalyst recovery

One of the most important and valuable factors in catalytic systems is the simple separation of the catalyst and the study of its reusability. In this regard, the reusability of Fe_3O_4@AMBA-CuI nanocatalyst in three-component reaction of heteroaryl halides with aryl or heteroaryl boronic acids and S_8 as sulfur source for the synthesis of **product 4a** was evaluated as a sample reaction. After the completion of the reaction, the Fe_3O_4@-AMBA-CuI nanocatalyst was readily recovered through magnetic separation, washed with ethanol absolute several times, and reused for next runs. As shown in Fig. 9, the Fe_3O_4@AMBA-CuI nanocatalyst can be reused at least six runs with constant catalytic activity. As shown in Fig. 10, VSM analysis showed that the recovered Fe_3O_4@AMBA-CuI catalyst (after 6 runs) has a magnetic property of 38.047 emu g^{-1}, which confirms that despite the separation and reusability of Fe_3O_4@AMBA-CuI nanocatalyst, it still has a high magnetic property. ICP-OES analysis was used to find out the amount of copper in the structure of the recovered Fe_3O_4@AMBA-CuI nanocatalyst after 6 runs, and the results showed that the amount of Cu in the structure of the nanocatalyst is 14.25×10^{-5} mol g^{-1}.

Comparison

To highlight the superior performance of the Fe_3O_4@AMBA-CuI nanocatalyst in comparison to previously documented catalytic systems, we opted to examine its efficacy in synthesis of 2-(phenylthio)benzo[*d*]as the model reaction. As depicted in Table 5, conventional methods in the literature often necessitated prolonged reaction times under harsh conditions, resulting in

Table 4 Scope of heteroaryl iodides and aryl or heteroaryl boronic acids for synthesis of heteroaryl-aryl and di-heteroaryl sulfides catalyzed by Fe$_3$O$_4$@AMBA-CuI nanomaterial[a]

Entry	Heteroaryl halide	Aryl boronic acid	Product (sulfide)
1			95% Product 4a
2			94% Product 4b
3			92% Product 4c
4			96% Product 4d
5			92% Product 4e

Table 4 (*Contd.*)
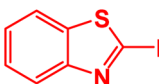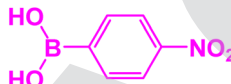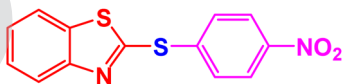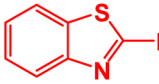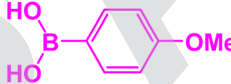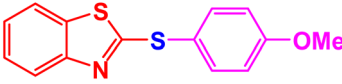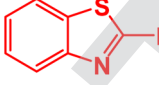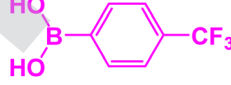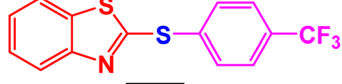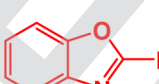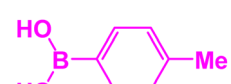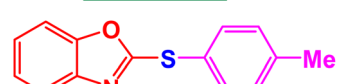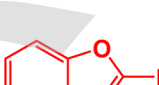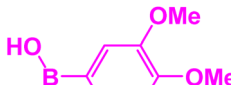
Heteroaryl—I + Ar—B(OH)₂ + S₈ → Heteroaryl—S—Ar

Conditions: (8 mol%) Fe₃O₄@AMBA-CuI, KOAc, PEG, 120 °C, 5 h

- **1**: Heteroaryl—I, 0.5 mmol
- **2**: S₈, 0.5 mmol
- **3**: Ar—B(OH)₂, 0.6 mmol

21 Examples; Yield: 84–97%; Products 4a–u

Heteroaryl: Benzothiazole, Benzoxazole, Benzimidazole, Oxadiazole, Benzofuran, imidazo[1,2-a]pyridine

Ar: Phenyl and Heteroaryl — **Heteroaryl**: Pyridine, Furan, Thiophene, Benzothiazole

Functional Groups on Phenyl Ring: Me, OMe, NO₂, CN, CF₃, H

Entry	Heteroaryl halide	Aryl boronic acid	Product (sulfide)
6	2-iodobenzothiazole	4-nitrophenylboronic acid	91% — Product 4f
7	2-iodobenzothiazole	4-methoxyphenylboronic acid	97% — Product 4g
8	2-iodobenzothiazole	4-(trifluoromethyl)phenylboronic acid	86% — Product 4h
9	2-iodobenzoxazole	4-methylphenylboronic acid	96% — Product 4i
10	2-iodobenzoxazole	3,4,5-trimethoxyphenylboronic acid	93% — Product 4j

Table 4 (*Contd.*)

Heteroaryl—I + Ar—B(OH)₂ + S₈ $\xrightarrow{\text{(8 mol%) Fe}_3\text{O}_4@\text{AMBA-CuI}, \text{KOAc, PEG, 120 °C, 5 h}}$ Heteroaryl—S—Ar

0.5 mmol **1**   0.5 mmol **2**   0.6 mmol **3**

21 Examples

Yield: 84–97%

Products 4a–u

Heteroaryl

Benzothiazole, Benzoxazole, Benzimidazole, Oxadiazole, Benzofuran, imidazo[1,2-*a*]pyridine

Ar:Phenyl and Heteroaryl   **Heteroaryl: Pyridine, Furan, Thiophene, Benzothiazole**

Functional Groups on Phenyl Ring : Me, OMe, NO₂, CN, CF₃, H

Entry	Heteroaryl halide	Aryl boronic acid	Product (sulfide)
11			91% Product 4k
12			85% Product 4l
13			92% Product 4m
14			86% Product 4n
15			84% Product 4o

Table 4 (*Contd.*)

Heteroaryl—I + Ar—B(OH)$_2$ → Heteroaryl—S—Ar

(8 mol%) Fe$_3$O$_4$@AMBA-CuI

KOAc, PEG, 120 °C, 5 h

1: 0.5 mmol
2: S$_8$ 0.5 mmol
3: 0.6 mmol

21 Examples
Yield: 84–97%
Products 4a-u

Heteroaryl

Benzothiazole, Benzoxazole, Benzimidazole, Oxadiazole, Benzofuran, imidazo[1,2-*a*]pyridine

Ar:Phenyl and Heteroaryl Heteroaryl: Pyridine, Furan, Thiophene, Benzothiazole

Functional Groups on Phenyl Ring : Me, OMe, NO$_2$, CN, CF$_3$, H

Entry	Heteroaryl halide	Aryl boronic acid	Product (sulfide)
16			88% — Product 4l
17			88% — Product 4q
18			90% — Product 4r
19			87% — Product 4s

Table 4 (*Contd.*)

Heteroaryl—I + Ar—B(OH)$_2$ → Heteroaryl—S—Ar

(8 mol%) Fe$_3$O$_4$@AMBA-CuI, KOAc, PEG, 120 °C, 5 h

1: 0.5 mmol; S$_8$ 2: 0.5 mmol; 3: 0.6 mmol

21 Examples; Yield: 84–97%; Products 4a–u

Heteroaryl: Benzothiazole, Benzoxazole, Benzimidazole, Oxadiazole, Benzofuran, imidazo[1,2-*a*]pyridine

Ar: Phenyl and Heteroaryl — **Heteroaryl:** Pyridine, Furan, Thiophene, Benzothiazole

Functional Groups on Phenyl Ring : Me, OMe, NO$_2$, CN, CF$_3$, H

Entry	Heteroaryl halide	Aryl boronic acid	Product (sulfide)
20			91% — Product 4t
21			92% — Product 4u

^{a} Yields referred to isolated sulfide products.

the product being synthesized with only moderate to good efficiency. In contrast, our approach utilized an environmentally friendly solvent and achieved the model reaction in just 5 hours, yielding the desired product with an outstanding efficiency of 95%. Furthermore, the Fe$_3$O$_4$@AMBA-CuI nanocatalyst demonstrated complete stability and adherence to the principles of green chemistry.

Conclusion

In this attractive and highly efficient, we shown that Fe$_3$O$_4$@-AMBA-CuI nanomaterial can be successfully catalyzed one-pot three-component reaction of heteroaryl halides with aryl or heteroaryl boronic acids and S$_8$ as sulfur source under eco-friendly conditions in order to synthesize heteroaryl-aryl and di-heteroaryl sulfides. Under this catalytic system, a broad spectrum of heteroaryl-aryl and di-heteroaryl sulfides were synthesized with high to excellent yields in less than 5 h. The reusability-experiments revealed that the Fe$_3$O$_4$@AMBA-CuI nanocatalyst can be magnetically separated and reused at least six runs without significant decrease in its catalytic

activity. VSM and ICP-OES analyzes confirmed that despite using the Fe$_3$O$_4$@AMBA-CuI nanocatalyst 6 times, the magnetic properties and stability of the catalyst were still maintained. Although all the obtained heteroaryl-aryl and di-heteroaryl sulfide products are known and previously reported, but synthesis of this number of heteroaryl-aryl and di-heteroaryl sulfides has never been reported by any methods.

Experimental

Synthesis of Fe$_3$O$_4$@AMBA-CuI nanocatalyst

At the first step the Fe$_3$O$_4$ was prepared according to previous report.[76] In the next step 1 g of Fe$_3$O$_4$ was dispersed in 50 mL of ethanol for 30 min and, then, 4 mmol of 3-amino-4-mercaptobenzoic acid (AMBA) was added to the reaction mixture and stirred under reflux conditions for 3 h. After the mixture was cooled, the synthesized Fe$_3$O$_4$@AMBA MNPs were accumulated using an external magnet, washed with water and ethanol and dried at 80 °C. Afterwards, 2 g of Fe$_3$O$_4$@AMBA was dispersed in 100 mL of ethanol for 30 minutes. Then, it was treated with 2.5 mmol of CuI and stirred under reflux
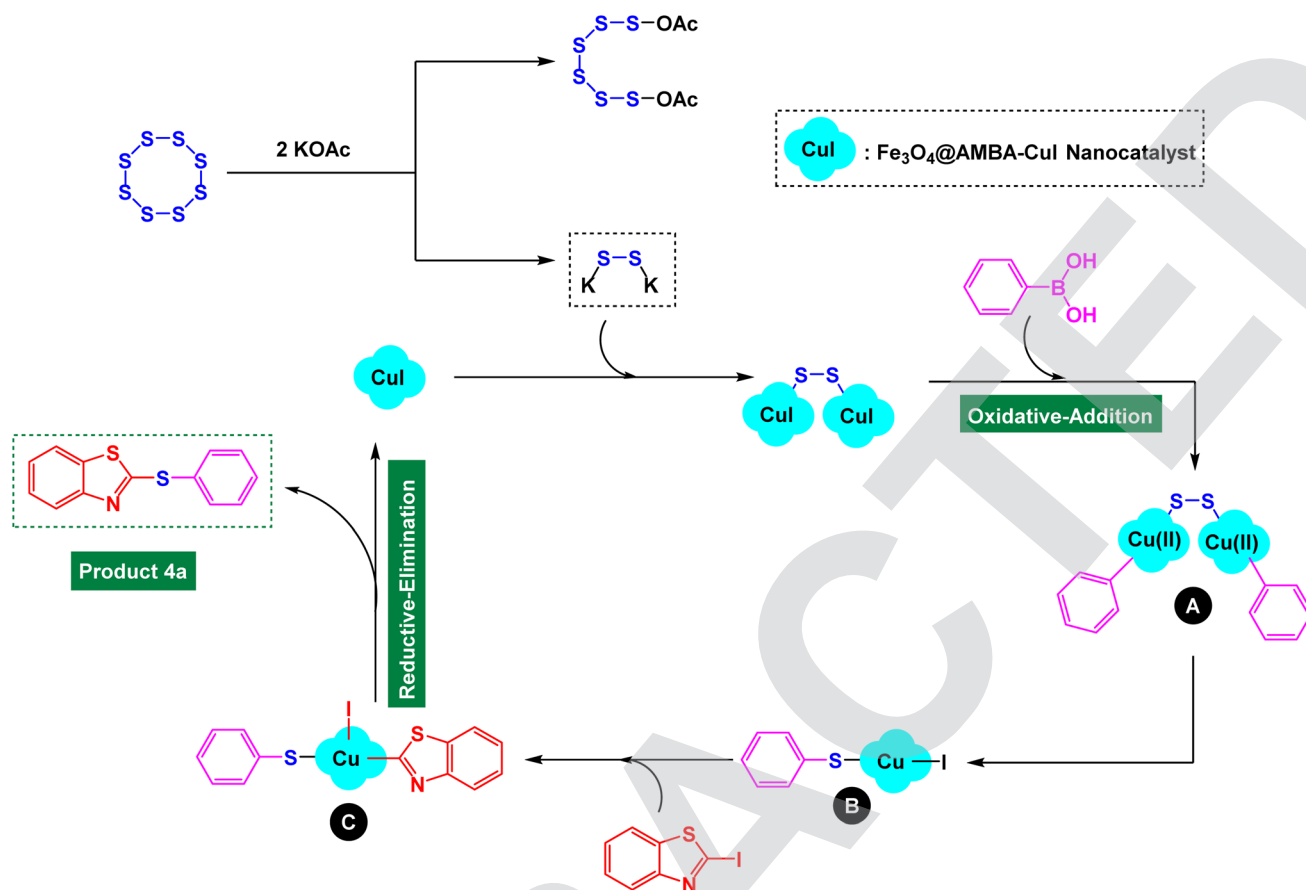
Scheme 2 Mechanistic pathway for synthesis of heteroaryl-aryl and di-heteroaryl sulfides through three-component reaction of heteroaryl halides with aryl or heteroaryl boronic acids and S_8 as sulfur source catalyzed by Fe_3O_4@AMBA-CuI nanomaterial.
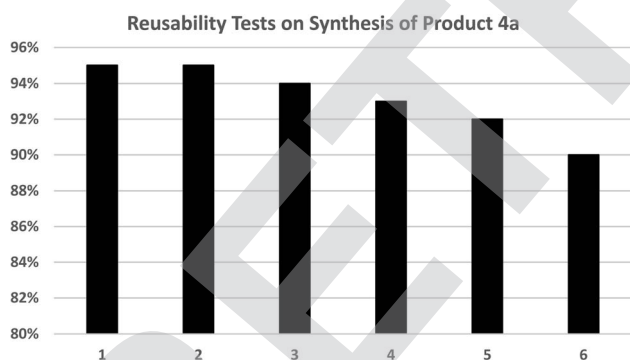

Fig. 9 Reusability rests of Fe_3O_4@AMBA-CuI nanocatalyst in preparation of 2-(phenylthio)benzo[d]thiazole (**Product 4a**).
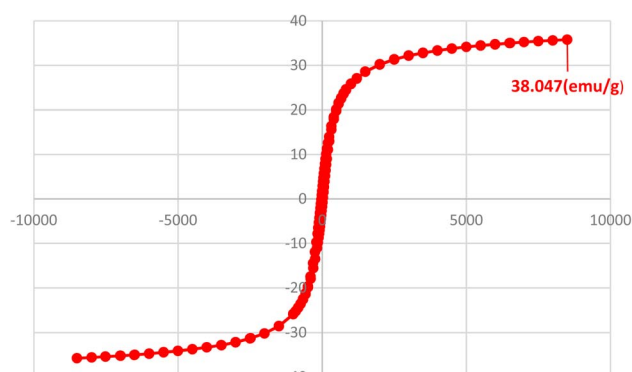

Fig. 10 VSM analysis of Fe_3O_4@AMBA-CuI nanocatalyst after 6 runs.

conditions for 8 h. The obtained [Fe_3O_4@ AMBA-CuI] complex was collected using an external magnet, washed using water and ethanol and, finally, dried at 80 °C (Scheme 1).

General procedure for preparation of heteroaryl-aryl and di-heteroaryl sulfides catalyzed by Fe_3O_4@AMBA-CuI nanocomposite

In a round bottomed flask, a mixture of heteroaryl iodides (0.5 mmol), aryl or heteroaryl boronic acids (0.6 mmol), S_8 (0.5 mmol) KOAc (2 equiv.) and Fe_3O_4@AMBA-CuI catalyst (8 mol%) was stirred in PEG-400 at 120 °C for 5 h (the progress of the reaction was monitored by thin-layer chromatography (TLC)). After completion of the reaction, the Fe_3O_4@AMBA-CuI was magnetically separated and reaction mixture was cooled to room temperature and H_2O (4 mL) was added. The product was extracted with EtOAc (3 × 4 mL) and dried over anhydrous Na_2SO_4. The crude material was purified with chromatography column on silica gel (EtOAc/n-hexane) give the heteroaryl-aryl

Table 5 Comparison of the activity of this method with reported methods for the preparation of 2-(phenylthio)benzo[d]thiazole (**product 4a**)

Entry	Catalytic system	Conditions	Yield (%) [Ref]
1	[NiCl$_2$(PPh$_3$)$_2$]	EtOH, reflux, 3 h	83%[71]
2	1,2-Diaminocyclohexane/CuI	DMSO. 90 °C, 4 h	86%[72]
3	1,10-Phenanthroline/CuI	1,4-Dioxane; rt → 90 °C; 12 h	76%[73]
4	Cationic 2,2′-bipyridyl/CoCl$_2$·6H$_2$O	Water, potassium hydroxide, zinc; 24 h, 100 °C	91%[74]
5	Fe$_3$O$_4$@AMBA-CuI	PEG-400, 120 °C, 5 h	95%[75]

and di-heteroaryl sulfides products with 84–97%. All heteroaryl-aryl and di-heteroaryl sulfides products are previously reported and known.[59,60,77–83] HNMR and CNMR were used in order to identify the structure of the heteroaryl-aryl and di-heteroaryl sulfide products.

## NMR data for heteroaryl-aryl and di-heteroaryl sulfide products

95%

Product 4a
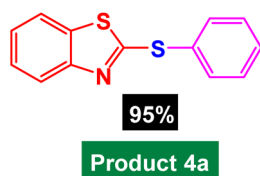
2-(Phenylthio)benzo[d]thiazole. Mp: 32–34 °C, ^{1}H NMR (500 MHz, CDCl$_3$) δ 8.06–8.02 (m, 2H), 7.64–7.60 (m, 2H), 7.58–7.46 (m, 5H); ^{13}C NMR (126 MHz, CDCl$_3$) δ 168.8, 155.0, 135.6, 135.1, 130.8, 130.4, 126.7, 124.5, 122.1, 120.7.


94%

Product 4b
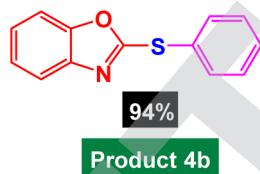
2-(Phenylthio)benzo[d]oxazole. Colorless oil, ^{1}H NMR (500 MHz, CDCl$_3$) δ 7.68–7.64 (m, 2H), 7.63–7.61 (m, 2H), 7.20–7.17 (m, 2H), 7.16–7.14 (m, 3H).; ^{13}C NMR (126 MHz, CDCl$_3$) δ 162.8, 152.3, 142.9, 135.1, 130.3, 129.9, 127.2, 124.7, 123.8, 119.4, 110.3.


92%

Product 4c
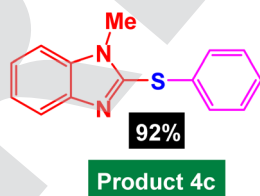
1-Methyl-2-(phenylthio)-1H-benzo[d]imidazole. Mp: 65–67 °C, ^{1}H NMR (500 MHz, CDCl$_3$) δ 7.61–7.57 (m, 2H), 7.48–7.45 (m, 2H), 7.38 (t, J = 4.3 Hz, 3H), 7.23–7.21 (m, 2H), 3.78 (s, 1H); ^{13}C NMR (126 MHz, CDCl$_3$) δ 146.5, 135.2, 131.5, 130.2, 129.8, 122.4, 118.6, 110.3, 32.9.


96%

Product 4d
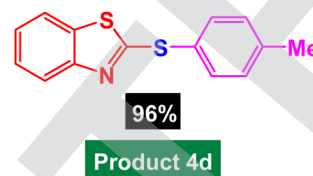
2-(p-Tolylthio)benzo[d]thiazole. Mp: 69–71 °C, ^{1}H NMR (500 MHz, CDCl$_3$) δ 7.81 (dd, J = 7.6, 1.2 Hz, 1H), 7.60–7.57 (m, 2H), 7.37–7.33 (m, 1H), 7.32–7.25 (m, 2H), 7.23–7.20 (m, 1H), 2.50 (s, 3H); ^{13}C NMR (126 MHz, CDCl$_3$) δ 165.3, 153.6, 135.9, 134.1, 130.5, 130.2, 129.7, 126.3, 124.2, 121.5, 120.8, 22.5.

92%

Product 4e
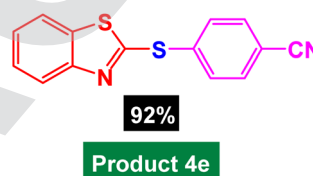
4-(Benzo[d]thiazol-2-ylthio)benzonitrile. Mp: 110–112 °C, ^{1}H NMR (500 MHz, CDCl$_3$) δ 7.88 (d, J = 7.7 Hz, 1H), 7.69–7.65 (m, 3H), 7.46–7.40 (m, 2H), 7.31 (d, J = 4.5 Hz, 1H), 7.29 (d, J = 4.6 Hz, 1H); ^{13}C NMR (126 MHz, CDCl$_3$) δ 167.2, 153.4, 136.5, 136.2, 135.7, 130.3, 128.5, 126.3, 124.6, 122.0, 120.1.

91%

Product 4f
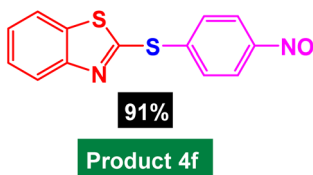
2-((4-Nitrophenyl)thio)benzo[d]thiazole. Mp: 86–89 °C, ^{1}H NMR (500 MHz, CDCl$_3$) δ 8.00–7.95 (m, 2H), 7.65–7.63 (m, 2H), 7.45–7.41 (m, 2H), 7.20–7.14 (m, 2H); ^{13}C NMR (126 MHz, CDCl$_3$) δ 161.1, 158.3, 142.8, 141.3, 139.5, 138.0, 130.2, 129.7, 128.6, 127.9, 118.4, 115.7.

98%
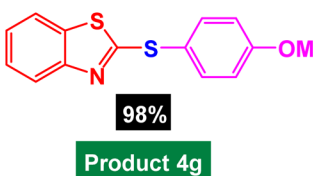
Product 4g

**2-((4-Methoxyphenyl)thio)benzo[d]thiazole.** Mp: 55–57 °C, ^{1}H NMR (500 MHz, CDCl$_3$) δ 7.84 (d, J = 7.6 Hz, 1H), 7.65–7.60

(m, 2H), 7.38–7.35 (m, 1H), 7.26 (d, J = 7.5 Hz, 1H), 7.22–7.00 (m, 3H), 3.89 (s, 3H); ^{13}C NMR (126 MHz, CDCl$_3$) δ 170.2, 161.0, 154.9, 137.6, 135.7, 126.12, 124.3, 121.5, 120.8, 120.2, 115.5.
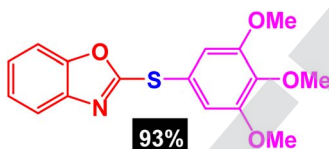

Product 4h — 86%

2-((4-(Trifluoromethyl)phenyl)thio)benzo[*d*]thiazole. Mp: 58–60 °C, ^{1}H NMR (500 MHz, CDCl$_3$) 8.02 (d, J = 7.8 Hz, 1H), 7.85 (d, J = 7.8 Hz, 3H), 7.69–7.65 (m, 2H), 7.64–7.60 (m, 1H), 7.59–7.57 (m, 1H); ^{13}C NMR (126 MHz, CDCl$_3$) δ 165.2, 141.0, 140.9, 139.5, 137.4, 136.5, 130.6, 129.7, 129.1, 128.7, 127.9, 127.3.
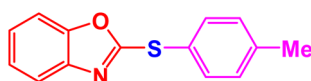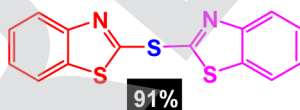

Product 4i — 96%

2-(*p*-Tolylthio)benzo[*d*]oxazole. Colorless oil, ^{1}H NMR (500 MHz, CDCl$_3$) δ 7.71 (d, J = 7.7 Hz, 2H), 7.61–7.55 (m, 2H), 7.31–7.24 (m, 2H), 7.21–7.18 (m, 2H), 2.54 (s, 3H); ^{13}C NMR (126 MHz, CDCl$_3$) δ 157.0, 155.2, 143.6, 141.5, 138.7, 130.5, 129.7, 127.3, 126.1, 120.3, 115.2, 22.5.

Product 4j — 93%
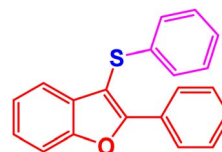
2-((3,4,5-Trimethoxyphenyl)thio)benzo[*d*]oxazole. Mp: 127–129 °C, ^{1}H NMR (500 MHz, CDCl$_3$) δ 7.85 (d, J = 8.3 Hz, 1H), 7.62 (d, J = 8.0 Hz, 1H), 7.43 (td, J = 7.7, 1.3 Hz, 1H), 7.26 (td, J = 7.5, 1.3 Hz, 1H), 7.10 (s, 2H), 3.85 (s, 6H), 3.64 (s, 3H); ^{13}C NMR (126 MHz, CDCl$_3$) δ 170.2, 155.3, 145.6, 141.2, 135.8, 130.7, 126.7, 125.3, 124.1, 121.0, 120.8, 58.9, 58.2.
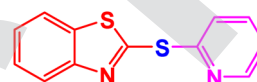

Product 4k — 91%

Bis(benzo[*d*]thiazol-2-yl)sulfane. Mp: 100–102 °C, ^{1}H NMR (500 MHz, CDCl$_3$) δ 7.85 (dd, J = 8.6 Hz, 2H), 7.65–7.60 (m), 7.45–7.40 (m, 4H); ^{13}C NMR (101 MHz, CDCl$_3$) δ 168.8, 141.6, 137.0, 135.9, 134.5, 130.2, 129.2, 127.3, 125.9.

Product 4l — 85%

2-Phenyl-3-(phenylthio)benzofuran. Mp: 66–68 °C, ^{1}H NMR (500 MHz, CDCl$_3$) δ 8.24 (dd, J = 8.3 Hz, 2H), 7.56 (d, J = 8.2 Hz, 1H), 7.48–7.41 (m, 5H), 7.37–7.23 (m, 5H), 7.22–7.16 (m, 1H); ^{13}C NMR (101 MHz, CDCl$_3$) δ 157.8, 153.2, 136.5, 130.6, 129.7, 129.4, 129.0, 128.7, 127.3, 126.5, 125.9, 125.4, 123.4, 120.5, 111.3, 104.9.

Product 4m — 92%

2-(Pyridin-2-ylthio)benzo[*d*]thiazole. Mp: 66–68 °C, ^{1}H NMR (500 MHz, CDCl$_3$) δ 9.26 (d, J = 1.8 Hz, 1H), 8.81 (dd, J = 4.9, 1.7 Hz, 1H), 8.29 (ddd, J = 8.1, 2.3, 1.8 Hz, 1H), 7.55–7.45 (m, 4H), 7.44 (ddd, J = 8.1, 4.9, 1.8 Hz, 1H); ^{13}C NMR (126 MHz, CDCl$_3$) δ 161.3, 154.6, 149.7, 136.5, 135.1, 132.5, 129.8, 128.9, 126.3, 122.4.
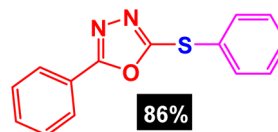
Product 4n — 86%

2-Phenyl-5-(phenylthio)-1,3,4-oxadiazole. Mp: 60–62 °C, ^{1}H NMR (500 MHz, CDCl$_3$) δ 7.91 (d, J = 7.6 Hz, 2H), 7.70–7.64 (m, 2H), 7.59 (t, J = 7.2 Hz, 1H), 7.49–7.42 (m, 5H); ^{13}C NMR (126 MHz, CDCl$_3$) δ 166.9, 166.1, 133.8, 132.4, 130.8, 130.2, 129.8, 127.6, 126.4, 123.9.
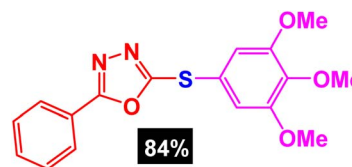
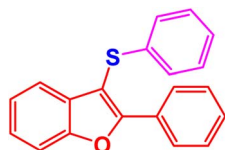**Product 4o** — 84%

2-Phenyl-5-((3,4,5-trimethoxyphenyl)thio)-1,3,4-oxadiazole. Mp: 140–142 °C, ^{1}H NMR (500 MHz, CDCl$_3$) δ 7.97 (d, J = 6.7 Hz, 2H), 7.52–7.50 (m, 3H), 6.95 (s, 2H), 3.97 (s, 9H); ^{13}C NMR (126 MHz, CDCl$_3$) δ 166.6, 163.9, 153.2, 140.3, 132.3, 130.0, 126.4, 123.7, 121.5, 111.3, 61.7, 55.5.

88%

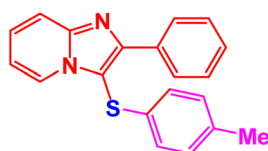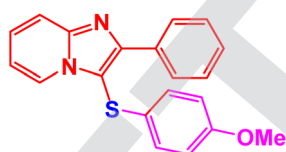**Product 4l**

2-Phenyl-3-(phenylthio)imidazo[1,2-*a*]pyridine. Mp: 92–94 °C, ^{1}H NMR (500 MHz, CDCl$_3$) δ 8.25 (d, 1H, J = 6.8 Hz), 8.18 (d, 2H, J = 7.6 Hz), 7.71 (d, 1H, J = 9.2 Hz), 7.45 (t, 2H, J = 7.7 Hz), 7.38 (d, 1H, J = 7.3 Hz), 7.30 (t, 1H, J = 8 Hz), 7.17 (t, 2H, J = 7.6 Hz), 7.11 (t, 1H, J = 7.6 Hz), 6.97 (d, 2H, J = 7.6 Hz), 6.85 (t, 1H, J = 6.7 Hz); ^{13}C NMR (126 MHz, CDCl$_3$) δ 151.0, 147.2, 133.5, 129.7, 128.5, 128.3, 127.4, 126.2, 125.6, 125.3, 124.5, 117.3, 112.2, 106.3.

88%

Product 4q

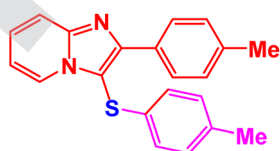**2-Phenyl-3-(*p*-tolylthio)imidazo[1,2-*a*]pyridine.** Mp: 135–137 °C, ^{1}H NMR (500 MHz, CDCl$_3$) δ 8.28 (d, 1H, J = 6.5 Hz), 8.21 (d, 2H, J = 7.5 Hz), 7.71 (d, 1H, J = 9.1 Hz), 7.46 (t, 2H, J = 7.6 Hz), 7.37 (d, 1H, J = 7.3 Hz), 7.28 (t, 1H, J = 8 Hz), 7.02 (d, 2H, J = 8 Hz), 6.95 (d, 2H, J = 8.1 Hz), 6.87 (t, 1H, J = 6.7 Hz), 2.38 (s, 3H); ^{13}C NMR (126 MHz, CDCl$_3$) δ 152.0, 145.3, 136.8, 133.5, 131.2, 130.7, 129.7, 128.6, 128.0, 126.4, 125.7, 117.9, 112.4, 106.3, 21.3.


90%

Product 4r

3-((4-Methoxyphenyl)thio)-2-phenylimidazo[1,2-*a*]pyridine. Mp: 112–114 °C, ^{1}H NMR (500 MHz, CDCl$_3$) δ 8.29 (d, 1H, J = 6.1 Hz), 8.22 (d, 2H, J = 8.2 Hz), 7.71 (d, 1H, J = 8.6 Hz), 7.42–7.40 (m, 2H), 7.35 (t, 1H, J = 5.7 Hz), 7.29–7.27 (m, 1H), 6.97 (d, 2H, J = 8.3 Hz), 6.85 (t, 1H, J = 5.6 Hz), 6.75 (d, 2H, J = 8.6 Hz), 3.70 (s, 3H).; ^{13}C NMR (126 MHz, CDCl$_3$) δ 158.6, 150.2, 146.7, 133.6, 130.9, 129.7, 128.8, 128.6, 127.7, 126.4, 125.7, 117.7, 115.9, 112.6, 107.4, 55.3.


87%

Product 4s

2-(*p*-Tolyl)-3-(*p*-tolylthio)imidazo[1,2-*a*]pyridine. Mp: 142–144 °C, ^{1}H NMR (500 MHz, CDCl$_3$) δ 8.24 (d, 1H, J = 6.8 Hz), 8.12 (d, 2H, J = 7.8 Hz), 7.70 (d, 1H, J = 9.1 Hz), 7.33 (t, 1H, J = 7.6 Hz), 7.25 (d, 2H, J = 8.3 Hz), 7.02 (d, 2H, J = 7.7 Hz), 6.92 (d, 2H, J = 7.7 Hz), 6.83 (t, 1H, J = 6.7 Hz), 2.38 (s, 3H), 2.25 (s, 3H).; ^{13}C NMR (126 MHz, CDCl$_3$) δ 151.1, 146.3, 138.7, 134.3, 130.7, 129.7, 129.1, 128.2, 126.4, 125.1, 124.4, 117.6, 112.7, 105.9, 21.3, 20.6.
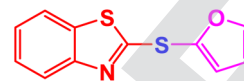
91%

Product 4t

2-(Furan-2-ylthio)benzo[*d*]thiazole. ^{1}H NMR (400 MHz, CDCl$_3$) δ 8.03 (dd, J = 8.5 Hz, 2H), 7.45 (d, J = 8.8 Hz, 2H), 6.99 (d, J = 8.7 Hz, 2H), 6.95 (d, J = 9.2 Hz, 1H); ^{13}C NMR (101 MHz, CDCl$_3$) δ 164.6, 161.7, 137.6, 130.5, 129.3, 119.1, 115.3, 114.5.
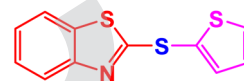
92%

Product 4u

2-(Thiophen-2-ylthio)benzo[*d*]thiazole. ^{1}H NMR (400 MHz, CDCl$_3$) δ 7.33–7.21 (m, 2H), 7.14–7.10 (m, 2H), 6.97–6.93 (m, 3H); ^{13}C NMR (101 MHz, CDCl$_3$) δ 168.3, 149.8, 135.0, 134.7, 132.1, 130.8, 130.2, 128.3, 117.6, 116.3, 115.4.

Conflicts of interest

There are no conflicts to declare.

References

1 S. Vajar and M. Mokhtary, *Polycyclic Aromat. Compd.*, 2019, **39**, 111–123.

2 M.-S. Shafik, *J. Synth. Chem.*, 2022, **1**, 132–136.

3 L. Kong and G. Liu, *Matter Radiat. Extremes*, 2021, 6, DOI: **10.1063/5.0071856**.

4 D. Yang, Y. Wang, C. Chen, Y. Su, L. Li, L. Miao, H. Gu, W. Zhao, L. Ding and D. Hu, *Inorg. Chem.*, 2023, **62**, 10408–10419.

5 Y. Zhang and N. Song, *Biol. Mol. Chem.*, 2023, **1**, 53–60.

6 Z. Song, D. Han, M. Yang, J. Huang, X. Shao and H. Li, *Appl. Surf. Sci.*, 2023, **607**, 155067.

7 R. Deilam, F. Moeinpour and F. S. Mohseni-Shahri, *Monatsh. Chem.*, 2020, **151**, 1153–1162.

8 X.-M. Wang, P. Zhang, Q. Xu, C.-Q. Guo, D.-B. Zhang, C.-J. Lu and R.-R. Liu, *J. Am. Chem. Soc.*, 2021, **143**, 15005–15010.

9 X. Zhao, Y. Zhang, Z. Hou and L. Wang, *Chin. J. Chem.*, 2023, **41**(22), 2963–2968.

10 L. Kong, Y. Liu, L. Dong, L. Zhang, L. Qiao, W. Wang and H. You, *Dalton Trans.*, 2020, **49**, 1947–1954.

11 M. Kazemi, *Nanomater. Chem.*, 2023, **1**, 1–11.

12 Q. Li, L. Xu and D. Ma, *Angew. Chem.*, 2022, **134**, DOI: **10.1002/ange.202210483**.

13 Z. Chen, T. Ma, Z. Li, W. Zhu and L. Li, *J. Mater. Sci. Technol.*, 2024, **179**, 198–207.

14 W. Wang, L. Cheng, H. Peng, W. Yao, R. Zhang, C. Chen and H. Cheng, *Chin. J. Org. Chem.*, 2019, **39**, 2851.

15 S. Paul, K. Pradhan, S. Ghosh, S. K. De and A. R. Das, *Adv. Synth. Catal.*, 2014, **356**, 1301–1316.

16 T. Mandal, *J. Synth. Chem.*, 2022, **1**, 8–15.

17 S. Gupta, *J. Synth. Chem.*, 2022, **1**, 16–21.

18 S. Gao, Q. Zhang, X. Su, X. Wu, X.-G. Zhang, Y. Guo, Z. Li, J. Wei, H. Wang, S. Zhang and J. Wang, *J. Am. Chem. Soc.*, 2023, **145**, 9520–9529.

19 Q. Zhang, S. Gao, Y. Guo, H. Wang, J. Wei, X. Su, H. Zhang, Z. Liu and J. Wang, *Nat. Commun.*, 2023, **14**, 1147.

20 S. A. Mousavi-Mashhadi and A. Shiri, *ChemistrySelect*, 2021, **6**, 3941–3951.

21 Z. Zhang, W. Zhang, Z.-W. Hou, P. Li and L. Wang, *J. Org. Chem.*, 2023, **88**, 13610–13621.

22 Q. Yu, *Sci. China Mater.*, 2023, **66**, 1079–1088.

23 P. Ghamari kargar, G. Bagherzade and H. Eshghi, *RSC Adv.*, 2020, **10**, 32927–32937.

24 M. Gholamhosseini-Nazari, S. Esmati, K. D. Safa, A. Khataee and R. Teimuri-Mofrad, *Res. Chem. Intermed.*, 2019, **45**, 1841–1862.

25 D. Chen, Q. Wang, Y. Li, Y. Li, H. Zhou and Y. Fan, *Chemosphere*, 2020, **247**, 125869.

26 M. Mohammadi, M. Khodamorady, B. Tahmasbi, K. Bahrami and A. Ghorbani-Choghamarani, *J. Ind. Eng. Chem.*, 2021, **97**, 1–78.

27 D. Tian, H. Zhou, H. Zhang, P. Zhou, J. You, G. Yao, Z. Pan, Y. Liu and B. Lai, *Chem. Eng. J.*, 2022, **428**, DOI: **10.1016/j.cej.2021.131166**.

28 Y. Zhu, Y. Liu, Q. Ai, G. Gao, L. Yuan, Q. Fang, X. Tian, X. Zhang, E. Egap, P. M. Ajayan and J. Lou, *ACS Mater. Lett.*, 2022, **4**, 464–471.

29 T. Tang, M. Zhou, J. Lv, H. Cheng, H. Wang, D. Qin, G. Hu and X. Liu, *Colloids Surf., B*, 2022, **216**, 112538.

30 Y. Zheng, Y. Liu, X. Guo, Z. Chen, W. Zhang, Y. Wang, X. Tang, Y. Zhang and Y. Zhao, *J. Mater. Sci. Technol.*, 2020, **41**, 117–126.

31 Z. Wang, C. Chen, H. Liu, D. Hrynshpan, T. Savitskaya, J. Chen and J. Chen, *Sci. Total Environ.*, 2020, **708**, 135063.

32 G. Meng, L. Zhen, S. Sun, J. Hai, Z. Zhang, D. Sun, Q. Liu and B. Wang, *J. Mater. Chem. A*, 2021, **9**, 24365–24373.

33 P.-B. Chen, J.-W. Yang, Z.-X. Rao, Q. Wang, H.-T. Tang, Y.-M. Pan and Y. Liang, *J. Colloid Interface Sci.*, 2023, **652**, 866–877.

34 S.-X. Mao, J.-Y. Song, W.-S. Zhu, H.-M. Li, J.-Y. Pang, D.-B. Dang and Y. Bai, *Fuel*, 2023, **352**, 128982.

35 S. Huang, J. Yuan, Y. Xie, K. Qing, Z. Shi, G. Chen, J. Gao, H. Tan and W. Zhou, *Cancer Nanotechnol.*, 2023, **14**, 43.

36 Y. Zhang, M. Zhao, J. Huang, N. Zhao and H. Yu, *Molecules*, 2023, **28**, 6671.

37 R. K. Sharma, S. Dutta, S. Sharma, R. Zboril, R. S. Varma and M. B. Gawande, *Green Chem.*, 2016, **18**, 3184–3209.

38 M. Kazemi, M. Ghobadi and A. Mirzaie, *Nanotechnol. Rev.*, 2018, **7**, 43–68.

39 S. Payra, A. Saha and S. Banerjee, *J. Nanosci. Nanotechnol.*, 2017, **17**, 4432–4448.

40 M. Kazemi, *Synth. Commun.*, 2020, **50**, 2095–2113.

41 J. Choi, A. Cho, J. H. Cho and B. M. Kim, *Appl. Catal., A*, 2022, **642**, 118709.

42 Z. Kheilkordi, G. Mohammadi Ziarani, F. Mohajer, A. Badiei and M. Sillanpää, *RSC Adv.*, 2022, **12**, 12672–12701.

43 L. Tang, F. Qin, F. Huang, D. Xu, Q. Hu and W. Zhang, *Appl. Organomet. Chem.*, 2022, **36**(7), e6723.

44 T. H. V. Kumar, J. Rajendran, R. Atchudan, S. Arya, M. Govindasamy, M. A. Habila and A. K. Sundramoorthy, *Environ. Res.*, 2023, **238**, 117193.

45 E. Tronc, C. Chanéac and J. P. Jolivet, *J. Solid State Chem.*, 1998, **139**, 93–104.

46 I. Khan, K. Saeed and I. Khan, *Arabian J. Chem.*, 2019, **12**, 908–931.

47 J. Rajendran, *J. Hazard. Mater.*, 2023, **449**, 130979.

48 P. So-ho, Y. Han-chul and J. Jae-chan, *Nanomater. Chem.*, 2023, **1**, 46–57.

49 Q. Wei, Z.-P. Wang, X. Zhang and Y. Zou, *J. Am. Chem. Soc.*, 2022, **144**, 9554–9558.

50 P. Anbarasan, H. Neumann and M. Beller, *Chem. Commun.*, 2011, **47**, 3233.

51 Z. Chen, S. M. Nasr, M. Kazemi and M. Mohammadi, *Mini-Rev. Org. Chem.*, 2020, **17**, 352–362.

52 L. Chen, A. Noory Fajer, Z. Yessimbekov, M. Kazemi and M. Mohammadi, *J. Sulfur Chem.*, 2019, **40**(4), 451–468.

53 M. Arisawa, T. Ichikawa and M. Yamaguchi, *Org. Lett.*, 2012, **14**, 5318–5321.

54 K. Takagi, *Chem. Lett.*, 1987, **16**, 2221–2224.

55 Z.-B. Dong, M. Balkenhohl, E. Tan and P. Knochel, *Org. Lett.*, 2018, **20**, 7581–7584.

56 J. Rafique, S. Saba, A. R. Rosário and A. L. Braga, *Chem. – Eur. J.*, 2016, **22**, 11854–11862.

57 Y. B. Bhujabal, K. S. Vadagaonkar, A. Gholap, Y. S. Sanghvi, R. Dandela and A. R. Kapdi, *J. Org. Chem.*, 2019, **84**, 15343–15354.

58 S. M. Allin, W. R. Bowman, R. Karim and S. S. Rahman, *Tetrahedron*, 2006, **62**, 4306–4316.

59 R.-Q. Luo, S. P. Guo, H.-L. Xiao and Q.-H. Li, *Tetrahedron*, 2022, **103**, 132564.

60 I. M. Yonova, C. A. Osborne, N. S. Morrissette and E. R. Jarvo, *J. Org. Chem.*, 2014, **79**, 1947–1953.

61 R. Zhang, H. Ding, X. Pu, Z. Qian and Y. Xiao, *Catalysts*, 2020, **10**, 1339.

62 C. C. Eichman and J. P. Stambuli, *Molecules*, 2011, **16**, 590–608.

63 N. Motahharifar, M. Nasrollahzadeh, A. Taheri-Kafrani, R. S. Varma and M. Shokouhimehr, *Carbohydr. Polym.*, 2020, **232**, DOI: **10.1016/j.carbpol.2019.115819**.

64 S. Rezayati, A. Ramazani, S. Sajjadifar, H. Aghahosseini and A. Rezaei, *ACS Omega*, 2021, **6**, 25608–25622.

65 N. Arsalani, H. Fattahi and M. Nazarpoor, *eXPRESS Polym. Lett.*, 2010, **4**, 329–338.

66 E. T. Tenório-Neto, T. Jamshaid, M. Eissa, M. H. Kunita, N. Zine, G. Agusti, H. Fessi, A. E. El-Salhi and A. Elaissari, *Polym. Adv. Technol.*, 2015, **26**, 1199–1208.

67 A. Abd Alkhalig Ahmed Bakheet, *Sci. J. Anal. Chem.*, 2017, **5**, 113.

68 M. Ma, Y. Yang, W. Li, R. Feng, Z. Li, P. Lyu and Y. Ma, *J. Mater. Sci.*, 2019, **54**, 323–334.

69 S. Hasan and E. Al-Bab, *Catalysts*, 2019, **9**, 839.

70 C. Perrino, E. Marconi, L. Tofful, C. Farao, S. Materazzi and S. Canepari, *Atmos. Environ.*, 2012, **54**, 36–43.

71 R. S. Barbiéri, C. R. Bellato, A. K. C. Dias and A. C. Massabni, *Catal. Lett.*, 2006, **109**, 171–174.

72 S. Murru, H. Ghosh, S. K. Sahoo and B. K. Patel, *Org. Lett.*, 2009, **11**, 4254–4257.

73 S. Murru, P. Mondal, R. Yella and B. K. Patel, *Eur. J. Org. Chem.*, 2009, **2009**, 5406–5413.

74 M.-T. Lan, W.-Y. Wu, S.-H. Huang, K.-L. Luo and F.-Y. Tsai, *RSC Adv.*, 2011, **1**, 1751.

75 P. Sharma, S. Rohilla and N. Jain, *J. Org. Chem.*, 2017, **82**, 1105–1113.

76 M. Aqeel Ashraf, Z. Liu, Y. Yang and D. Zhang, *Synth. Commun.*, 2020, **50**, 2885–2905.

77 P. Gandeepan, J. Mo and L. Ackermann, *Chem. Commun.*, 2017, **53**, 5906–5909.

78 M. Vaddamanu, K. Velappan and G. Prabusankar, *New J. Chem.*, 2020, **44**, 129–140.

79 X. Liu, S.-B. Zhang, H. Zhu and Z.-B. Dong, *J. Org. Chem.*, 2018, **83**, 11703–11711.

80 H.-A. Du, X.-G. Zhang, R.-Y. Tang and J.-H. Li, *J. Org. Chem.*, 2009, **74**, 7844–7848.

81 L.-F. Niu, Y. Cai, C. Liang, X.-P. Hui and P.-F. Xu, *Tetrahedron*, 2011, **67**, 2878–2881.

82 S. Hu, S. Du, Y. Yao, Z. Yang, H. Ren and Z. Chen, *Synlett*, 2019, **30**, 625–629.

83 X. Li, T. Yuan, Y. Yang and J. Chen, *Tetrahedron*, 2014, **70**, 9652–9660.